

Thouless Conductances of a Three-Dimensional Quantum Hall System

Chao Zheng,^{1,*} Kun Yang,² and Xin Wan^{1,3}

¹*Zhejiang Institute of Modern Physics, Zhejiang University, Hangzhou 310027, China*

²*Physics Department and National High Magnetic Field Laboratory,
Florida State University, Tallahassee, FL 32306, USA*

³*CAS Center for Excellence in Topological Quantum Computation,
University of Chinese Academy of Sciences, Beijing 100190, China*

(Dated: November 25, 2021)

We investigate the longitudinal conductances of a disordered three-dimensional (3D) quantum Hall system within a tight-binding lattice model using numerical Thouless conductance calculations. We find that different from the 2D case, the 3D quantum Hall system exists a finite range of extended states in each subband. Within this range, the longitudinal conductance along the magnetic field (z axis) behaves like a quasi-1D normal metal, while the longitudinal conductance perpendicular to the magnetic field is controlled by layered conducting states stacked coherently. Inside the quantum Hall gap, we study the novel 2D chiral surface states at the sidewalls of the sample. We demonstrate the metal-insulator crossover of the surface states in the z direction by modifying the interlayer hopping strength and disorder strength. The typical behaviors of the Thouless conductance and the wave function of the surface states in quasi-1D metal and insulator regimes are investigated. Further, in order to predict the regime of the surface states for arbitrary parameters, we determine an explicit relationship between the localization length of surface states and the microscopic parameters of the model.

I. INTRODUCTION

The quantum Hall effect (QHE) in two-dimensional (2D) electron systems originates from discrete Landau levels forming under a strong perpendicular magnetic field^{1,2}. While the physical picture underlying QHE seems specific to 2D, the generalization of the QHE to 3D systems has also been considered³⁻⁶. The most straightforward way to construct a 3D QHE is to stack 2D QHE layers along the magnetic field (z axis), as long as the coupling strength is small compared to the 2D quantum Hall gap, we expect the QHE still exists. There are also other schemes to realize a 3D QHE, such as by virtue of spontaneous charge (spin) density wave^{3,7} or based on topological semimetals⁸. In the present work, we focus on the first one.

The distinct feature of a 2D quantum Hall system is its chiral edge states, which are immune to disorder. In the 3D case, the chiral edge state of each layer is coupled to neighboring edge states, forming a 2D chiral surface state⁶. In the presence of disorder, this 2D surface state remains ballistic perpendicular to the magnetic field, however, parallel to the magnetic field in a mesoscopic sample, there exist three distinct regimes of transport, namely, 2D chiral metal, quasi-1D metal, and quasi-1D insulator⁹⁻¹⁴.

Experimentally, the 3D QHE was first put forward by Störmer *et al.*⁴ in an engineered multi-quantum well system. The existence of the 2D chiral surface state in this system was further confirmed in Ref.¹⁵. For real materials, anisotropic layered 3D materials are the most promising candidates to host the 3D QHE. Signatures of 3D QHE have been found in Bechgaard salts^{16,17}, η -Mo₄O₁₁¹⁸, graphite^{19,20}, n -doped Bi₂Se₃²¹, EuMnBi₂²², and most recently, ZrTe₅⁷ and BaMnSb₂²³. Remarkably, the last one provides the first observation of the 2D chiral surface states in a real material. These materials offer us great opportunities to study the 3D QHE and its novel surface states.

Previous theoretical works on both the 3D QHE and

its surface states are mainly investigated within a network model^{5,11-14,24}. The network model is based on the semi-classical picture of electrons in a strong magnetic field and smooth disorder potential^{25,26}. It neglects the inter-Landau level scattering and deals with transmission probability amplitudes instead of wave functions^{5,26}. An alternative way to describe the 3D quantum Hall system is by using a tight-binding model. So far, however, there have been very few investigations of this model in the literature²⁷.

Motivated by recent experimental developments in this direction, in this work, we investigate the longitudinal conductances of a disordered 3D quantum Hall system within a *tight-binding lattice model* using numerical Thouless conductance calculations. We begin by stacking the 2D QHE layers along the z direction, for small interlayer hoppings, we find that the peak conductance of lowest subband in the x direction scales linear with the number of layers, while in the z direction, it is inversely proportional to the number of layers. From the size dependence of conductances at weak disorder, we find that the 3D quantum Hall system exists a finite range of extended states in each subband. As disorder increases, the conductance peak of the lowest subband in the x direction floats to the central subband as in the 2D case, while there is no clear evidence of floating in the z direction. We thus conclude that for extended states, the longitudinal conductance in the z direction behaves like a quasi-1D normal metal, while the longitudinal conductance in the x direction is controlled by layered conducting states stacked coherently. Inside the gap, the system is a 3D quantized Hall conductor, the system is insulating in the bulk but hosts 2D surface states at its sidewalls. By modifying the interlayer hopping strength and disorder strength, we demonstrate the metal-insulator crossover of the novel 2D chiral surface states in our model. The typical behaviors of the Thouless conductance and the wave function of the surface states in quasi-1D metal and insulator regimes are investigated. Finally, in order to predict the regime of the surface states for arbitrary parameters, we give an explicit relation-

ship between the localization length of surface states and the microscopic parameters of the model.

The rest of the paper is organized as follows. In Sec. II we describe the Hamiltonian for 3D quantum Hall system and introduce the numerical Thouless conductance method. In Sec. III we present our numerical results. The paper is summarized in Sec. IV.

II. MODELS AND METHODS

A. 3D lattice model

We consider an electron on an $L_x \times L_y \times L_z$ cubic lattice in the presence of a magnetic field $B\hat{z}$ with tight-binding Hamiltonian

$$\mathcal{H} = - \sum_{\langle i,j \rangle} \left(t_{ij} e^{i\theta_{ij}} c_i^\dagger c_j + h.c. \right) + \sum_i \epsilon_i c_i^\dagger c_i, \quad (1)$$

where we have anisotropic nearest-neighboring hopping

$$t_{ij} = \begin{cases} 1 & i \text{ and } j \text{ are horizontal nearest neighbors,} \\ t_z & i \text{ and } j \text{ are vertical nearest neighbors,} \\ 0 & i \text{ and } j \text{ are not nearest neighbors.} \end{cases}$$

We choose Landau gauge $\vec{A} = (0, Bx, 0)$ and define $\theta_{ij} = \frac{e}{\hbar} \int_i^j \vec{A} \cdot d\vec{l}$. The magnetic flux ϕ per unit cell in a horizontal plane is

$$\frac{\phi}{\phi_0} = \frac{Ba^2}{hc/e} = \frac{1}{2\pi} \sum_{\square} \theta_{ij}, \quad (2)$$

where $\phi_0 = hc/e$ is the flux quantum, and the disorder potential ϵ_i are independent variables with identical uniform distribution on $[-W/2, W/2]$.

In the 2D limit with $L_z = 1$, the clean model has a butterfly-like self-similar energy spectrum, as the flux ϕ per unit cell varies. When the flux ϕ per unit cell is chosen as ϕ_0/N for integer N , there are exactly N subbands in the spectrum. The side subbands have Chern number +1 each and can be regarded as broadened Landau levels. The lowest subband, whose localization length is moderate, is suitable for studying the universal behavior of quantum Hall transitions in the presence of disorder. For small t_z , the subband gaps may not close by the dispersion in z axis, so the Hall conductance in the horizontal direction remains quantized.

Figure 1 shows the evolution of density of states, at $W = 2-5$, for a system with $L = 24$, $\phi = \phi_0/3$, and $t_z = 0.1$. The gaps between the subbands close at about $W = 3$. For the small t_z , we find the density of states is very similar to that of the corresponding 2D lattice as expected.

B. Thouless Conductance

The longitudinal conductance of a finite system can be related to the sensitivity of eigenenergies to changes in the

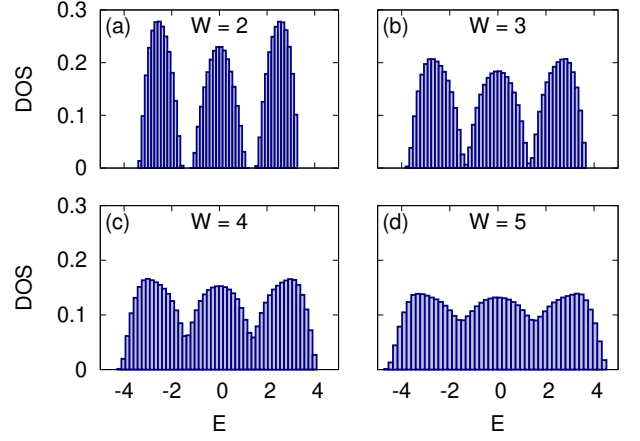


FIG. 1. Density of states of a $24 \times 24 \times 24$ cubic lattice with $\phi = \phi_0/3$ and $t_z = 0.1$ for (a) $W = 2$, (b) $W = 3$, (c) $W = 4$, and (d) $W = 5$.

boundary conditions. The idea came from D. J. Thouless, who argued that the shift in energies of eigenstates due to boundary condition change should be of the order of $\delta E \sim \hbar/\tau$, where $\tau \sim L^2/D$ is the time that takes for an electron to diffuse to the boundary²⁸. The diffusion constant D can be related to the longitudinal conductance by the Einstein relation,

$$\sigma_{xx} = e^2 D \rho, \quad (3)$$

where ρ is the density-of-states at the Fermi energy E_F . Therefore, the sensitivity can be quantified in a dimensionless way²⁹

$$g_{xx} = \frac{\langle \delta E \rangle}{\langle \Delta E \rangle} \sim \frac{\hbar}{e^2} \sigma_{xx}, \quad (4)$$

where $\langle \delta E \rangle$ is the average shift in the energy level due to a change of boundary conditions along x direction, and $\langle \Delta E \rangle = 1/L^2 \rho$ the mean energy level separation. Ando showed that the Thouless number can be applied to 2D systems in a strong magnetic field, and obtained

$$\sigma_{xx} = A \frac{e^2}{h} g_{xx}, \quad A = \frac{\pi}{2} \quad (5)$$

for peak conductivity for spin-polarized electrons³⁰. In numerical calculation, the value of g_L depends on the detailed method to evaluate the energy shift. In general, the proportionality constant A is expected to be of order unity.

As system size increases, the Thouless conductance of a localized state decreases to zero exponentially, while that of a metallic state does not decrease, or decrease slowly to a finite value due to finite-size corrections. Therefore, the Thouless number can be used to distinguish metallic states from localized states. Since quantum Hall transition is a special kind of metal-insulator transition, the peak Thouless conductance of a single Landau level is expected to be a universal constant, related to the longitudinal conductivity³¹.

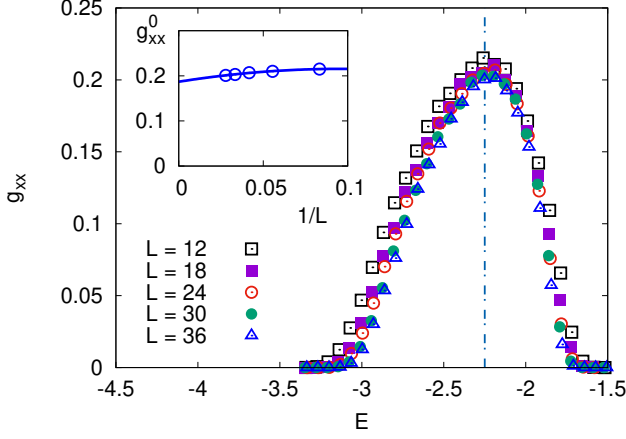


FIG. 2. In-plane Thouless conductance g_{xx} of the lowest subband in an $L \times L$ square lattice with $\phi = \phi_0/3$ and $W = 2$. The vertical line at $E = -2.25$ indicates the location of the peak of g_{xx} . Inset shows the peak conductance as a function of $1/L$, which converges to $g_{xx}^0 = 0.187 \pm 0.002$ in the thermodynamics limit.

In this study, we define $\langle \delta E \rangle$ as the arithmetic average of the energy curvature in the boundary-condition space. Because the time-reversal symmetry is broken in the model, we calculate the curvature in the vicinity of the periodic boundary conduction. For small systems, the calculation of curvature for random boundary conditions helps suppress the artefacts due to van Hove singularities.

To determine the prefactor A in Eq. (5) that relates Thouless conductance to longitudinal conductance, we consider the 2D case. For small disorder $W = 2$, the lowest subband in the case of $\phi = \phi_0/3$ describes a single disorder-broadened Landau level. As shown in the inset of Fig. 2, the peak Thouless conductance decreases slowly with system size and can be fit by

$$g_{xx}^0 = 0.187 + 0.60L^{-1} - 3.1L^{-2}. \quad (6)$$

In the thermodynamic limit the peak value converges to $g_{xx}^0 = 0.187 \pm 0.002$. The value corresponds to $\sigma_{xx} = 0.5e^2/h$ at a quantum Hall plateau transition. So in our calculation, we estimate $A = 2.67 \pm 0.03$.

III. RESULTS

A. Evolution of the lowest subband from 2D to 3D

We start by stacking 24×24 square lattices along the magnetic field \vec{B} to a 3D lattice. In the absence of vertical hopping, the longitudinal conductance perpendicular to \vec{B} scales with the number of layers, while the longitudinal conductance parallel to \vec{B} is zero. We turn on the vertical hopping to $t_z = 0.1$, still small compared to the horizontal hopping $t = 1$. To study the crossover from 2D to 3D, we compare the conductance for $L_z = 1, 2, 3, 4, 6, 8, 12$, and 24. For the 3D system, we calculate Thouless conductance g_{xx} along the

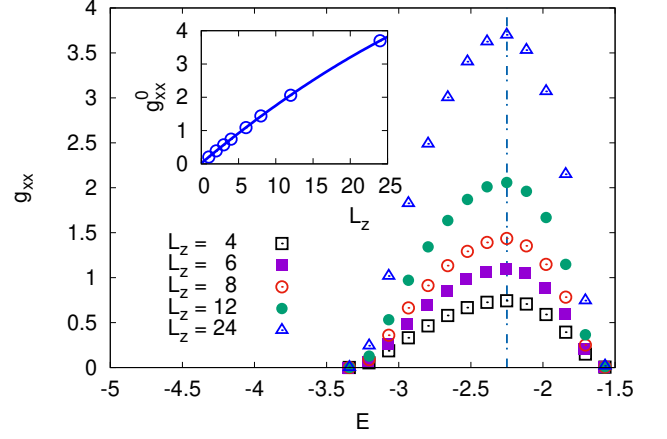


FIG. 3. Thouless conductance g_{xx} , perpendicular to the magnetic field, of the lowest subband in a $24 \times 24 \times L_z$ cubic lattice with $\phi = \phi_0/3$, $W = 2$ and $t_z = 0.1$. The vertical line at $E = -2.25$ indicates the location of the peak of g_{xx} . Inset shows the peak conductance g_{xx}^0 as a function of L_z , which can be fit by $g_{xx}^0(L_z) = 0.020 + 0.188L_z - 0.00143L_z^2$ up to the cubic case $L_z = 24$.

x -axis by changing the boundary conditions along the x direction and, similarly, g_{zz} by changing the boundary conditions along the z direction.

Figure 3 plots Thouless conductance along the x direction for the same lowest subband in the case of $\phi = \phi_0/3$ and $W = 2$. Due to the increasing number of layers, the number of states in the lowest subband increases. But the subband width barely changes because of the small hopping amplitude in the z direction. While the shape of g_{xx} is not changed by increasing L_z , the peak conductance g_{xx}^0 changes. We find the $g_{xx}^0(L_z)$ can roughly be fit by

$$g_{xx}^0(L_z) = 0.020 + 0.188L_z - 0.00143L_z^2, \quad (7)$$

for L_z up to 24, when $L_x = L_y = 24$. The coefficient of the quadratic term is small and can be neglected for $L_z \leq 12$. Neglecting the quadratic corrections and the small constant, the fit suggests that each layer contributes $g_{xx}^0 = 0.188 \pm 0.001$, which is identical to the contribution in an isolated layer within error bars.

We now turn to Thouless conductance along the z direction, along which the magnetic field aligns and the hopping is weak. Like g_{xx} , the vertical Thouless conductance develops a hump, whose shape remains unchanged as L_z increases. But unlike g_{xx} , the peak conductance g_{zz}^0 decreases with L_z , and our power-law fit to

$$g_{zz}^0(L_z) = g_0 L_z^{-\alpha}, \quad (8)$$

gives $\alpha = 0.983 \pm 0.015$, which suggests that g_{zz}^0 is inversely proportional to L_z within error bars.

We note that the peak of the lowest band in the density of states is located around $E_p = -2.66$, which coincides with the peak of g_{zz} , but not g_{xx} , which peaks around $E_p^{(x)} = -2.25$. There is no shift of peak in either g_{zz} or g_{xx} , as L_z

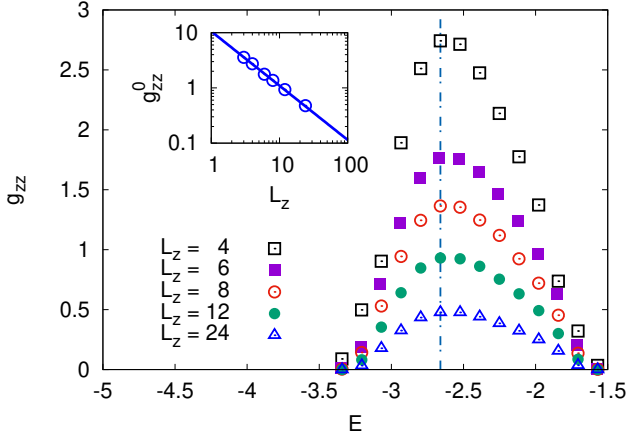


FIG. 4. Thouless conductance g_{zz} , parallel to the magnetic field, of the lowest subband in a $24 \times 24 \times L_z$ cubic lattice with $\phi = \phi_0/3$, $W = 2$ and $t_z = 0.1$. The vertical line at $E = -2.66$ indicates the location of the peak of g_{zz} . Inset shows the peak conductance g_{zz}^0 as a function of L_z , which can be fit by $g_{zz}^0(L_z) = 10.6 L_z^{-0.983}$.

increases from 1 to 24. At $E_p = -2.66$, the peak g_{zz} is inversely proportional to L_z , indicating the system is in a metallic phase. The shift, or floating, of the g_{xx} peak is expected to originate from the floating of extended states in the 2D limit³², as we will discuss more in the following subsection as disorder increases. It also suggests that the g_{xx} in the multilayer cases is dominated by conducting states in each 2D layer. The deviation of g_{xx}^0 from linear behavior suggests that the coherence of extended states along the z axis plays a role in the longitudinal conductance in the x - y plane.

In the 2D case, there is only one critical energy in the lowest subband, at which we find extended states even in the thermodynamic limit. When Fermi energy moves across the critical energy, an integer quantum Hall plateau transition occurs. This, however, is quite different from the 3D case, where a range of metallic states exist; in fact, we already see that the peaks of g_{xx} and g_{zz} differ. To estimate the energy range for the metallic phase at $W = 2.0$, we explore the finite-size effect of the conductances for the cubic lattice with $L_x = L_y = L_z = L$. Figure 5 plot both g_{xx} and g_{zz} as a function of energy for the lower half of the spectrum. We choose, here, $\phi = \phi_0/3$, $t_z = 0.1$, and $W = 2.0$ as before. The size dependence of the Thouless conductance along two perpendicular directions remains to be the same, although we can clearly identify two insulating regimes and two metallic regimes, separated by $E = -3.20$, -1.62 , and -1.05 , as indicated by dot-dashed lines in Fig. 5. The mobility edges found here is consistent with the result of the transfer matrix method in Ref.²⁷. We note that the phase at $-1.62 < E < -1.05$, which includes the band gap, is accompanied by the quantization of Hall conductance and is, therefore, a quantized Hall insulator. We will explore the phase in greater detail in the following subsections.

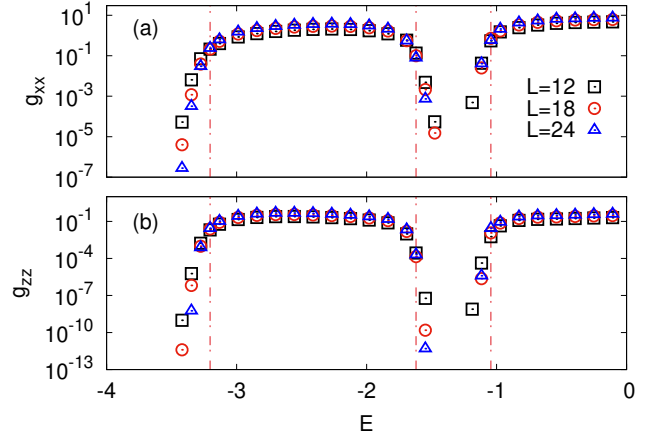


FIG. 5. Thouless conductance (a) g_{xx} , perpendicular to the magnetic field and (b) g_{zz} , parallel to the magnetic field, of the lowest subband and a half of the central band in an $L \times L \times L$ cubic lattice with $\phi = \phi_0/3$, $t_z = 0.1$, and $W = 2.0$ for $L = 12, 18, 24$. The vertical lines at $E = -3.20, -1.62$, and -1.05 indicate the locations of mobility edge, as the size dependence of both g_{xx} and g_{zz} differs on the two sides of the energies. The lines define four different phases along the horizontal axis. The phases from left to right are insulator, metal, quantized Hall insulator, and metal, respectively.

B. Disorder effects in the bulk

So far, we find that for a relatively small disorder $W = 2.0$ energy states in most of the lowest subband are in a metallic phase. But the phase differs from a normal metallic one. Based on the bulk Thouless conductance, we can argue that the longitudinal conductance along the magnetic field \vec{B} behaves like that of a quasi-1D normal metal. The longitudinal conductance perpendicular to \vec{B} is controlled by layered conducting states stacked coherently. We now focus on $L \times L \times L$ cubic samples and study the Thouless conductances along x and z directions. In particular, we are interested in the manifestation of the quantized Hall phase as disorder varies.

Figure 6(a) shows g_{xx} for the lowest subband and part of the central subband in the case of $\phi = \phi_0/3$ and $L = 24$ for $W = 2-5$. As disorder increases, the conductance peak of the lowest subband floats to the central subband, as found in the 2D case³². No peak can be identified for the lowest subband at $W = 5$, as it merges with the central subband. In the 3D case we find that, before the merge, the peak value g_{xx}^0 increases linearly as L increases from 12 to 24, which is consistent with metallic behavior.

Similarly, we compare g_{zz} for various W with $L = 24$ in Figure 6(b). The distinct feature of g_{zz} is that the deep dip separating the lowest subband and the central subband persists to $W = 5$, when the two subbands are not resolvable in g_{xx} . There is also no clear evidence of the floating of the g_{zz} peak of the lowest subband, in contrast to that of g_{xx}^0 , as we have commented in the previous subsection. The peak value g_{zz}^0 also scales linearly with L , showing metallic behavior for the range of disorder strength we consider. Fig. 6(c) plots g_{zz}^0 as a function of $1/W$ for various L . The curves can be fit by

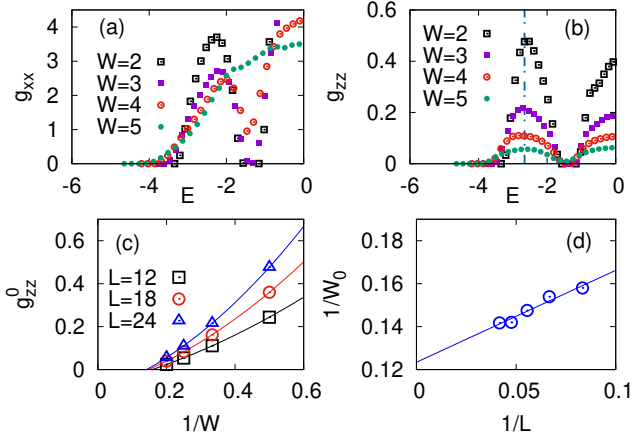


FIG. 6. (a) Thouless conductance g_{xx} and (b) Thouless conductance g_{zz} of the lowest subband and a half of the central band in an $L \times L \times L$ cubic lattice with $\phi = \phi_0/3$, $t_z = 0.1$, and $L = 24$ for $W = 2-5$. The dot-dashed line indicates the peak of g_{zz}^0 as mentioned in Fig. 4. (c) Peak conductance g_{zz}^0 as a function of $1/W$ for various L . We fit the data by quadratic curves with horizontal intercepts $1/W_0(L)$. (d) The dependence of $1/W_0$ as a function of $1/L$, which can be extrapolated to $L \rightarrow \infty$ at $1/W_0 = 0.123 \pm 0.003$.

quadratic functions, which have size-dependent horizontal intercepts $1/W_0(L)$. This is an indication of a metal-insulator transition at the band center at sufficiently small $1/W$, or sufficiently large W . We plot the intercept $1/W_0$ against $1/L$ and fit the data by a straight line, which has a vertical intercept $1/W_0 = 0.123 \pm 0.003$. In other words, when disorder strength is greater than $W_c = 8.1 \pm 0.2$, we expect that the system shows insulating behavior at the peak location of g_{zz} , or $E = -2.66$ as we have obtained earlier.

Note that we have discussed two methods to detect the boundaries of the metallic phase of the lattice model. In Fig. 5, we have analyzed the dependence of g_{xx} and g_{zz} on system size, from which we can extract the mobility edge. This approach is expected to be more effective at small disorder, where the phase boundaries in the phase diagram in the W - E plane depend weakly on the disorder. On the other hand, in Fig. 6, we have first studied the dependence of g_{zz} on disorder strength for a given system size and extrapolate the characteristic disorder that suppresses g_{zz} to zero. We have then carried out the finite-size scaling of the characteristic disorder to extract the critical disorder in the thermodynamic limit. This method is expected to work more effectively at large disorder, where the phase boundary in the phase diagram in the W - E plane is almost flat as energy changes.

C. Chiral surface states

Our main interest so far has been focused on the metallic behavior and the metal-insulator transition of the 3D system. Another interesting transport property is, however, associated with the surface of a 3D quantum Hall system. This phase is located at the gap region between the lowest subband and the

central subband, characterized by a Chern number 1 for each layer perpendicular to the magnetic field. With open boundary conditions as in real experimental situations, the chiral edge state of each layer is coupled to neighboring edge states, forming a chiral surface state.

The transport properties of this chiral surface state is highly anisotropic in the presence of disorder⁶. Perpendicular to the magnetic field, due to the chiral nature of the edge states, the transport is ballistic with a velocity v . Parallel to the magnetic field, the localization effect is suppressed by the unidirectional transport in the x direction. In order to make quantum interference happen, an electron has to circumnavigate the sample and return to its starting point. This can never happen in an infinite sample. Therefore, it has been argued that for an infinite sample, the transport along the z direction is always diffusive, regardless of the disorder strength⁶. Using the Einstein relation, we can obtain the conductivity of the 2D sheet in the z direction:

$$\sigma_{zz} = e^2 \rho D = \frac{D}{v} \frac{e^2}{h} = \sigma \frac{e^2}{h}, \quad (9)$$

where D is the diffusion constant, $\rho = 1/hv$ the density of states, $\sigma = D/v$ the dimensionless conductivity.

Interestingly, for a mesoscopic sample, depending on its vertical sheet conductivity σ_{zz} , the circumference C , and the height L_z , there are three distinct regimes of transport in the z direction connected by universal crossovers, namely, 2D chiral metal, quasi-1D metal, and quasi-1D insulator⁹⁻¹⁴. The time needed for an electron to circle around the sample is $\tau = C/v$. Within this time, the electron will diffuse a distance

$$L_0 = \sqrt{D\tau} = \sqrt{DC/v} \quad (10)$$

in the z direction. If $L_z \ll L_0$, then the system is a 2D chiral metal. In this circumstance, the electron diffuses out of the sample without a complete round-trip of the circumference.

For finite C with very long L_z , the system is of quasi-1D nature, we expect the surface state is localized along the z direction. Typically, the localization length ξ of such quasi-1D system is proportional to its 1D conductivity, which can be written as:

$$\xi = 2C\sigma = 2DC/v. \quad (11)$$

For $L_0 \ll L_z \ll \xi$, the system is a quasi-1D conductor, in this case, the electron circles around the sample many times before diffusing out. For $L_z \gg \xi$, the interference effect becomes dominant, finally turns the system into a quasi-1D insulator.

For our lattice model, the diffusion constant D of the surface state in the z direction depends on the interlayer hopping strength t_z , disorder strength W and the ballistic velocity v of the edge states. By adopting the result derived in the 2D chiral surface model^{6,33}, we have

$$D \propto \frac{t_z^2}{W^2} v \quad (12)$$

for our 3D model. Substituting Eq. (12) into Eq. (10) and (11), we have:

$$L_0 \propto \sqrt{\frac{t_z^2}{W^2} C}, \quad (13)$$

$$\xi \propto \frac{t_z^2}{W^2} C. \quad (14)$$

Thus both L_0 and ξ only depend on t_z , W and C , they are independent of v .

Below, we demonstrate the metal-insulator crossover of the surface state within our 3D lattice model, by fixing the dimensions of the system, only changing t_z and W . We note that to enter into the 2D chiral metal regime, one requires $L_z \ll L_0$. To increase L_0 , we can simply increase t_z and decrease W , but that also tends to drive the system into the ballistic regime. Another way to increase L_0 is to increase C , but due to the square root in Eq. (13), the system size needed is numerically quite challenging for the Thouless conductance calculation^{13,14}, thus we only focus on the quasi-1D metal and insulator regimes in the following sections.

1. Quasi-1D metal

We first present the results in the quasi-1D metal regime. To study the surface state, we apply open boundary conditions to the x and y directions and calculate Thouless conductance g_{zz} in the z direction. Figure 7(a) shows g_{zz} of the lowest subband and a half of the central band in a $21 \times 21 \times L_z$ cubic lattice with $\phi = \phi_0/3$, $t_z = 0.2$ and $W = 1.3$. g_{zz} develops plateaus inside the spectral gaps of the system, which are the contributions from the surface states. We show an enlarged view of this region in the inset of Fig. 7(a). In Fig. 7(b), we plot the plateau value g_{zz}^s at $E = -1.36$ as a function of system height L_z . The log-log plot suggests a power-law decrease of g_{zz}^s with respect to L_z , which can be fit to

$$g_{zz}^s(L_z) = g_0 L_z^{-\alpha}, \quad (15)$$

with $\alpha = 0.926 \pm 0.031$. This "ohmic" dependence of conductance suggests that the system is a conductor in the z direction.

The transport behavior is determined by the localization properties of the wave function. In Fig. 7(c) and (d), we plot the wave function in a $21 \times 21 \times 21$ cubic lattice at $E = -1.36$ for a specific disorder configuration. One can find that the wave function is extended over the whole sheath of the sample, indicating its conducting nature.

2. Quasi-1D insulator

The quasi-1D insulator regime can be achieved by decreasing the interlayer hopping strength t_z and increasing the disorder strength W , this is demonstrated in Fig. 8, in which $\phi = \phi_0/3$, $t_z = 0.04$ and $W = 2$. In Fig. 8(a), we show the height dependence of g_{zz} in a $21 \times 21 \times L_z$ cubic lattice, note that we use semi-log coordinate here. Since a quasi-1D system approximately favors a log-normal curvature distribution in the localization regime, here we use geometric averages for $\langle \delta E \rangle$ ³⁴. We plot the plateau value g_{zz}^s at $E = -1.36$ as a function of L_z in Fig. 8(b), the semi-log plot clearly shows an exponential decay of g_{zz}^s with L_z , indicating it is an insulator

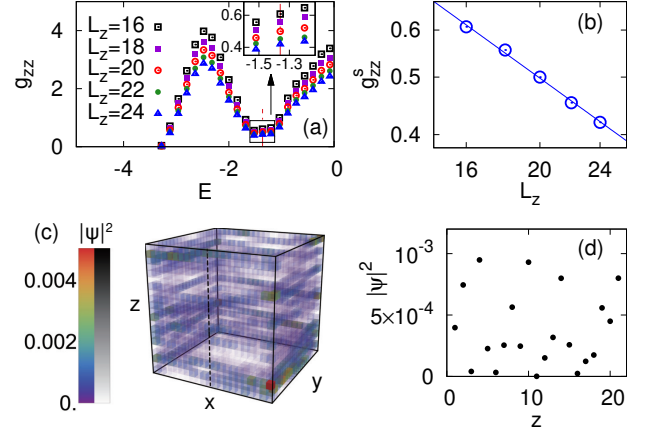


FIG. 7. Thouless conductance g_{zz} and wave function of the surface state in the 1D metallic regime with $\phi = \phi_0/3$, $t_z = 0.2$ and $W = 1.3$. (a) Thouless conductance g_{zz} of the lowest subband and a half of the central band in a $21 \times 21 \times L_z$ cubic lattice with open boundary conditions along x and y directions. Inset shows a zoom-in view around the plateau region inside the spectral gaps. (b) Log-log plot of the plateau value g_{zz}^s at $E = -1.36$ [indicated as the vertical dot-dashed line in (a)] as a function of L_z , which can be fit by $g_{zz}^s(L_z) = 7.97 L_z^{-0.926}$. (c) The probability density $|\psi|^2$ for a particular disorder realization in a $21 \times 21 \times 21$ cubic lattice at $E = -1.36$. The result is obtained by exact diagonalization under open boundary conditions in the x and y directions and periodic boundary condition in the z direction. Each lattice point is represented by a small cube, whose color and opacity depends on the value of $|\psi|^2$. The color and opacity bar is given on the left of the plot. (d) shows the probability density $|\psi|^2$ along the dashed vertical line in (c).

in the z direction. An explicit exponential fit to

$$g_{zz}^s(L_z) = g_0 e^{-L_z/\xi}, \quad (16)$$

gives a localization length $\xi = 2.24 \pm 0.07$. We notice that ξ is about $1/10$ of L_z , thus we are deep in the localization regime in the present case.

In Fig. 8(c), we show a 3D plot of the wave function at $E = -1.36$ in a $21 \times 21 \times 21$ cubic lattice for a particular disorder realization. In this case, the surface state is concentrated to a few layers in the z direction. Figure 8(d) plots the probability density along the dashed vertical line in (c). One can obtain the localization length from wave function by using an exponential fit:

$$|\psi(z)|^2 = |\psi_0|^2 e^{-2|z-z_0|/\xi}, \quad (17)$$

where z_0 is the maximum position of $|\psi|^2$. The fit yields $\xi = 1.77 \pm 0.13$ for the left wing and $\xi = 2.13 \pm 0.26$ for the right wing of the wave function, which is roughly consistent with the result from the Thouless conductance.

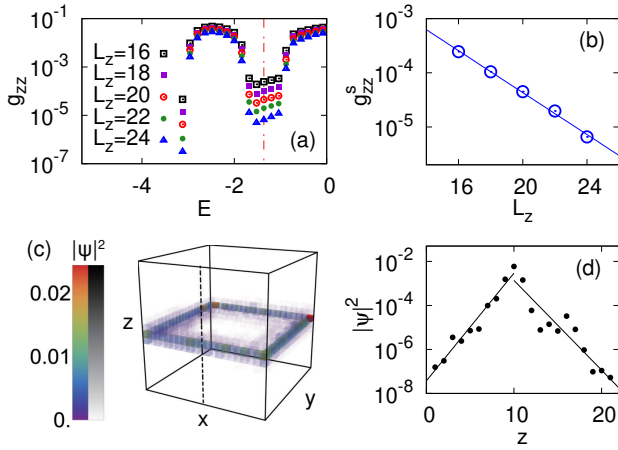


FIG. 8. Thouless conductance g_{zz} and wave function of the surface state in the 1D localized regime with $\phi = \phi_0/3$, $t_z = 0.04$ and $W = 2$. (a) Semi-log plot of Thouless conductance g_{zz} in a $21 \times 21 \times L_z$ cubic lattice with open boundary conditions along x and y directions. (b) Semi-log plot of the plateau value g_{zz}^s at $E = -1.36$ [indicated as the vertical dot-dashed line in (a)] as a function of L_z , which can be fit by $g_{zz}^s(L_z) = 0.320e^{-L_z/2.24}$. (c) The probability density $|\psi|^2$ for a particular disorder realization in a $21 \times 21 \times 21$ cubic lattice at $E = -1.36$, plotted in the same way of Fig. 7(c). (d) shows the semi-log plot of probability density $|\psi|^2$ along the dashed vertical line in (c). The fit to the wings with an exponential decay $e^{-2z/\xi}$ yields $\xi = 1.77 \pm 0.13$ for the left wing and $\xi = 2.13 \pm 0.26$ for the right wing.

3. Determining the relationship between localization length and the microscopic parameters of the model

So far, we explore the surface states using two specific sets of parameters which belong to quasi-1D metal and insulator, respectively. For arbitrary parameters, in order to determine the regime of the system, we need to compare the localization length ξ with system height L_z . As already mentioned above, the localization length depends on the interlayer hopping strength t_z , disorder strength W , and the circumference C of the system [see Eq. (14)]. We are now in a position to verify Eq. (14) numerically. In the end, we are able to predict the regime of the system for arbitrary parameters.

To do this, we repeat the procedure in Sec. III C 2, and determine the localization length from the height dependence of Thouless conductance in an $L \times L \times L_z$ cubic lattice. The sets of parameters we choose and the final result is shown in Fig. 9. We find that the localization length ξ indeed has a linear dependence on $(t_z^2/W^2)C$, which can be fit by:

$$\xi = 53.2 \frac{t_z^2}{W^2} C + 0.363. \quad (18)$$

Now we can use Eq. (18) to estimate the localization length under various parameters. For example, using the parameters for the quasi-1D metal in Sec. III C 1, the calculated localization length is $\xi = 106$, which is about five times the size of L_z , indicating we are indeed in the metallic regime. We note that special care is required when applying Eq. (18) to

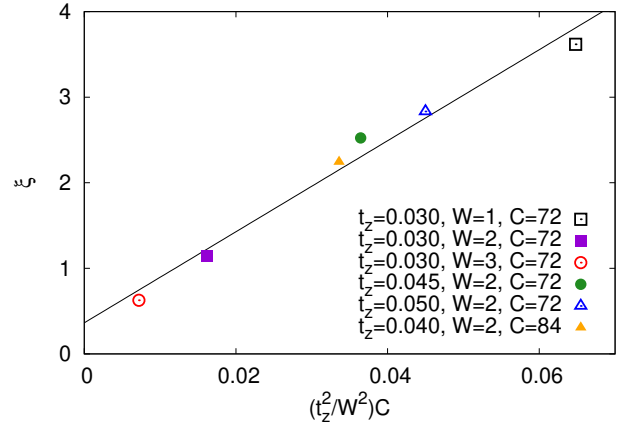


FIG. 9. Relationship between localization length ξ of the surface states and the microscopic parameters of the model. We determine the localization length from the height dependence of Thouless conductance g_{zz} in an $L \times L \times L_z$ cubic lattice, in the same way of Fig. 8. Here C is the circumference of the sample, which equals $4L$ in the present case. The localization length ξ has a linear dependence on $(t_z^2/W^2)C$.

systems with large t_z or W , since the (mobility) gaps may already close in that case, thus a well-defined surface state does not exist.

IV. SUMMARY AND DISCUSSION

In summary, we have investigated the longitudinal conductances of a disordered 3D quantum Hall system within a tight-binding lattice model using numerical Thouless number calculations. In particular, by stacking the 2D QHE layers along the z direction, we find that the 3D quantum Hall system exists a finite range of extended states in each subband at small disorder, different from the 2D case. Within this range, the longitudinal conductance along the magnetic field g_{zz} behaves like a quasi-1D normal metal, while the longitudinal conductance perpendicular to the magnetic field is controlled by layered conducting states stacked coherently. As disorder increases, the conductance peak of g_{xx} of the lowest subband floats to the central subband as in the 2D case, while there is no clear evidence of floating of g_{zz} . Inside the quantum Hall gap, we demonstrate the metal-insulator crossover of the novel 2D chiral surface states in the z direction by modifying the interlayer hopping strength t_z and disorder strength W . In real experiments, these can be achieved by uniaxial stress and disorder doping, respectively. The typical behaviors of the Thouless conductance and the wave function of the surface states in quasi-1D metal and insulator regimes are presented. In order to predict the regime of the surface states for arbitrary parameters, we give an explicit relationship between the localization length of surface states and the microscopic parameters of the model.

Besides the very recent work of Ref.²³, the only experimental realization of the 2D chiral surface states is the en-

gineered multi-quantum well system¹⁵. However, since the sample sizes are much larger than the phase coherence lengths in the experiment, only an incoherent 2D chiral metal has been studied^{13,15,35}. So far, the three regimes of phase-coherent transport have not been investigated in the experiments. Recently discovered anisotropic layered 3D materials thus offer a unique opportunity to study both the 3D QHE and its novel 2D chiral surface states. Samples with dimensions smaller than the phase coherence length are highly desired in the future. We mention that for such small samples, in addition to transport measurement, real-space probe techniques such as scanning tunneling microscopy can also be a useful tool to detect the metal-insulator crossover of the surface states, as

demonstrated in Figs. 7 and 8 in the paper.

V. ACKNOWLEDGEMENTS

The work at Zhejiang University was supported by the National Natural Science Foundation of China through Grant No. 11674282 and the Strategic Priority Research Program of Chinese Academy of Sciences through Grant No. XDB28000000. KY's work was supported by the National Science Foundation Grant No. DMR-1932796, and performed at the National High Magnetic Field Laboratory, which is supported by National Science Foundation Cooperative Agreement No. DMR-1644779, and the State of Florida.

* zhengchaonju@gmail.com

- ¹ S. D. Sarma and A. Pinczuk, *Perspectives in Quantum Hall Effects: Novel Quantum Liquids in Low-Dimensional Semiconductor Structures* (Wiley, New York, 1997).
- ² R. Prange, M. Cage, K. Klitzing, S. Girvin, A. Chang, F. Duncan, M. Haldane, R. Laughlin, A. Pruisken, and D. Thouless, *The Quantum Hall Effect*, Graduate Texts in Contemporary Physics (Springer, New York, 2012).
- ³ B. I. Halperin, *Jpn. J. Appl. Phys.* **26**, 1913 (1987).
- ⁴ H. L. Störmer, J. P. Eisenstein, A. C. Gossard, W. Wiegmann, and K. Baldwin, *Phys. Rev. Lett.* **56**, 85 (1986).
- ⁵ J. T. Chalker and A. Dohmen, *Phys. Rev. Lett.* **75**, 4496 (1995).
- ⁶ L. Balents and M. P. A. Fisher, *Phys. Rev. Lett.* **76**, 2782 (1996).
- ⁷ F. Tang, Y. Ren, P. Wang, R. Zhong, J. Schneeloch, S. A. Yang, K. Yang, P. A. Lee, G. Gu, Z. Qiao, *et al.*, *Nature (London)* **569**, 537 (2019).
- ⁸ C. M. Wang, H.-P. Sun, H.-Z. Lu, and X. C. Xie, *Phys. Rev. Lett.* **119**, 136806 (2017).
- ⁹ L. Balents, M. P. Fisher, and M. R. Zirnbauer, *Nucl. Phys. B* **483**, 601 (1997).
- ¹⁰ H. Mathur, *Phys. Rev. Lett.* **78**, 2429 (1997).
- ¹¹ I. A. Gruzberg, N. Read, and S. Sachdev, *Phys. Rev. B* **55**, 10593 (1997).
- ¹² I. A. Gruzberg, N. Read, and S. Sachdev, *Phys. Rev. B* **56**, 13218 (1997).
- ¹³ S. Cho, L. Balents, and M. P. A. Fisher, *Phys. Rev. B* **56**, 15814 (1997).
- ¹⁴ V. Plerou and Z. Wang, *Phys. Rev. B* **58**, 1967 (1998).
- ¹⁵ D. P. Druist, P. J. Turley, K. D. Maranowski, E. G. Gwinn, and A. C. Gossard, *Phys. Rev. Lett.* **80**, 365 (1998).
- ¹⁶ J. R. Cooper, W. Kang, P. Auban, G. Montambaux, D. Jérôme, and K. Bechgaard, *Phys. Rev. Lett.* **63**, 1984 (1989).
- ¹⁷ S. T. Hannahs, J. S. Brooks, W. Kang, L. Y. Chiang, and P. M. Chaikin, *Phys. Rev. Lett.* **63**, 1988 (1989).
- ¹⁸ S. Hill, S. Uji, M. Takashita, C. Terakura, T. Terashima, H. Aoki, J. S. Brooks, Z. Fisk, and J. Sarrao, *Phys. Rev. B* **58**, 10778 (1998).
- ¹⁹ Y. Kopelevich, J. H. S. Torres, R. R. da Silva, F. Mrowka, H. Kempa, and P. Esquinazi, *Phys. Rev. Lett.* **90**, 156402 (2003).
- ²⁰ B. A. Bernevig, T. L. Hughes, S. Raghu, and D. P. Arovas, *Phys. Rev. Lett.* **99**, 146804 (2007).
- ²¹ H. Cao, J. Tian, I. Miotkowski, T. Shen, J. Hu, S. Qiao, and Y. P. Chen, *Phys. Rev. Lett.* **108**, 216803 (2012).
- ²² H. Masuda, H. Sakai, M. Tokunaga, Y. Yamasaki, A. Miyake, J. Shiogai, S. Nakamura, S. Awaji, A. Tsukazaki, H. Nakao, *et al.*, *Sci. Adv.* **2**, e1501117 (2016).
- ²³ J. Liu, J. Yu, J. Ning, L. Miao, L. Min, K. Lopez, Y. Zhu, H. Yi, T. Pillsbury, Y. Zhang, *et al.*, *arXiv:1907.06318* (2019).
- ²⁴ Z. Wang, *Phys. Rev. Lett.* **79**, 4002 (1997).
- ²⁵ J. T. Chalker and P. D. Coddington, *J. Phys. C* **21**, 2665 (1988).
- ²⁶ B. Kramer, T. Ohtsuki, and S. Kettemann, *Phys. Rep.* **417**, 211 (2005).
- ²⁷ X. R. Wang, C. Y. Wong, and X. C. Xie, *Phys. Rev. B* **59**, R5277 (1999).
- ²⁸ D. Thouless, *Phys. Rep.* **13**, 93 (1974).
- ²⁹ D. C. Licciardello and D. J. Thouless, *J. Phys. C* **8**, 4157 (1975).
- ³⁰ T. Ando and H. Aoki, *J. Phys. Soc. Jpn* **54**, 2238 (1985).
- ³¹ Y. Huo, R. E. Hetzel, and R. N. Bhatt, *Phys. Rev. Lett.* **70**, 481 (1993).
- ³² K. Yang and R. N. Bhatt, *Phys. Rev. Lett.* **76**, 1316 (1996).
- ³³ J. J. Betouras and J. T. Chalker, *Phys. Rev. B* **62**, 10931 (2000).
- ³⁴ G. Casati, I. Guarneri, F. M. Izrailev, L. Molinari, and K. Życzkowski, *Phys. Rev. Lett.* **72**, 2697 (1994).
- ³⁵ D. Druist, K.-H. Yoo, P. Turley, E. Gwinn, K. Maranowski, and A. Gossard, *Superlattices Microstruct.* **25**, 181 (1999).